Dynamic Coupling Map: Acceleration Space Analysis for Underactuated Robots

Ziad Zamzami and Faiz Ben Amar

Sorbonne Universites, UPMC Paris VI, Institut Systèmes Intelligents et de Robotique,
ISIR - CNRS UMR 7222, Boite courrier 173, 4 Place JUSSIEU, 75252, Paris, France

Abstract: Swing-up and throwing tasks for underactuated manipulators are examples of dynamic motions that exhibit highly nonlinear coupling dynamics. One of the key ingredients for such complex behaviors is motion coordination to exploit their passive dynamics. Despite the existence of powerful tools such as nonlinear trajectory optimization, they are usually treated as blackboxes that provide local optimal trajectories. We introduce the Dynamical Coupling Map (DCM), a novel graphical technique, to help gain insight into the output trajectory of the optimization and analyze the capability of underactuated robots. The DCM analysis is demonstrated on the swing up motion of a simplified model of a gymnast on high bar. The DCM shows in a graphical and intuitive way the pivotal role of exploiting the nonlinear inertial forces to reach the unstable equilibrium configuration while taking into account the torque bounds constraints. In this paper, we present the DCM as a posteriori analysis of a local optimal trajectory, found by employing the direct collocation trajectory optimization framework.

1 INTRODUCTION

Humans and animals are capable of overcoming complex terrain challenges with graceful and agile movements. One of the key ingredients for such complex behaviors is motion coordination to exploit natural dynamics. Sports performers coordinate their action in many different ways to achieve their goals. Coordination is a key feature from the graceful, precise action of an ice dancer to the explosive, physical power of a triple jumper. Lizard coordinate its tail swing to stabilize its dynamic motion over rough terrain (Libby et al., 2012). Cheetah can rapidly accelerate and maneuver during the pursuit of its prey by the coordinating of the motion of its tail (Patel and Braae, 2013). Understanding and emulating these motions is the one of the long-standing grand challenges in robotics and biomechanics,with possible applications in rehabilitation, sport, search-and-rescue, environmental monitoring and security.

Unlike conventional fully-actuated manipulators where the natural dynamics can be suppressed by classical feedback control techniques, a large and diverse array of dynamical systems falls under the class of underactuated systems. The unactuated nature gives rise to many interesting control problems which require fundamental non-linear approaches (Spong, 1998). Underactuated systems are defined as mechanical systems in which the dimension of the configuration space exceeds that of the control input space, i.e. fewer control inputs than the available degrees of freedom. Such restriction can be the result of 1)an actuator failure (Arai et al., 1998); 2) intentional choice of a minimalist design which leads to a less costly, lighter and more compact machine; 3) rigid robots with elastic joints or flexible links (Spong, 1998); 4) or even imposed by the nature of the system itself such as non-prehensile manipulation (Lynch and Mason, 1996) and recently extended to legged robots as floating base systems (Wieber Pierre-Brice, Tedrake Russ, 2015).

Synthesizing motion behavior for such underactuated systems is quite challenging. Underactuation impose constraints on their dynamics that restrict the family of trajectories their configurations and accelerations can follow. These constraints are second-order nonholonomic constraints (Wieber, 2005)(Nagarajan et al., 2013). Moreover, cannot be fully feedback linearized (Spong, 1995). Underacuated system can only be controlled indirectly either through contact forces with the environment or through inertial forces which rises from the nonlinear inertial coupling of the

articulated system (Tamegaya et al., 2008), in this paper we focus on the latter.

(Hauser and Murray, 1990) introduced a canonical model of underactuated systems known as the Acrobot (for acrobatic robot) introduced by (Hauser and Murray, 1990). It can be considered is a highly simplified model of a human gymnast on the high bar, where the underactuated first joint models the gymnast's hands on the bar, and the actuated second joint models the gymnast's hips. The objective is to swing up the Acrobot from the downward stable equilibrium point to the upright unstable equilibrium point and balance it about the upright vertical. This motion control problem is usually decomposed into two subproblems; first, the swing-up motion control (Åström and Furuta, 2000) (Spong, 1995) (Xin, 2013), once the robot's configuration is brought up to the neighborhood of the unstable equilibrium point, switching to a stabilization controller is necessary(Olfati-Saber, 2001). Several variants of the Acrobot have been proposed either increasing the number of degrees of freedoms (Kurazume and Hasegawa, 2002) (Shkolnik and Tedrake, 2008) (Ibuki et al., 2015) or by varying the placement of the actuators (Luca and Oriolo, 2002). For the sake of illustration, we focus in this paper, on an extended version of the acrobat called the gymnast introduced by (Xin and Kaneda, 2007b) arguing the importance of a third active joint representing the shoulder.

During the last two decades, many researchers have investigated the approach of passivity or energy-based control of underactuated mechanical systems. (Lam and Davison, 2006) showed that the coupling becomes more complex when the number of links increases, and its control problem becomes more challenging. (Xin and Kaneda, 2007a) noted that energy based techniques are difficult to apply for higher dimension robots.

1.1 Approach and Contribution

In this work, we employ nonlinear trajectory optimization for the swing-up motion generation and control. Second-order Nonholonomic and torque constraints fit naturally into the direct formulation of trajectory optimization. Furthermore, there exists strong evidence that humans solve task-level and motor-level challenges though optimization processes. A good overview of optimal control in sensorimotor systems is given by (Todorov, 2004).

Trajectory optimization approach is becoming increasingly attractive with the advent of computational power and the recent advances in nonlinear optimiza-
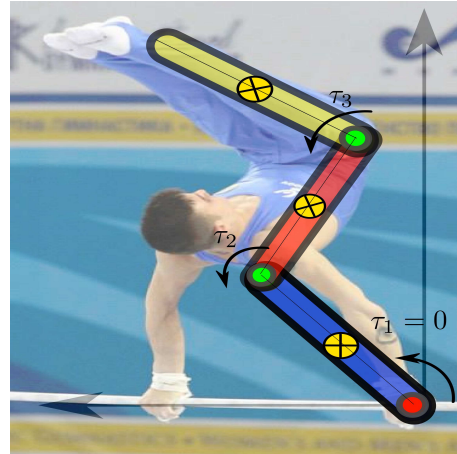
Figure 1: Simplified model of a gymnast on a high bar.
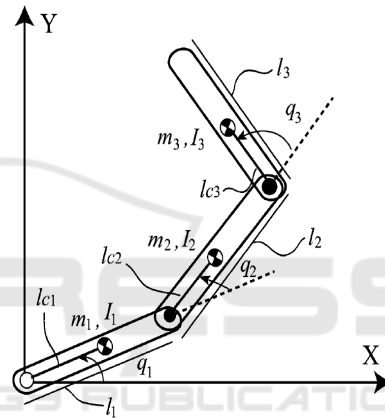
Figure 2: 3-link Gymnast model of underactuated mechanical system with passive joint at the base.

tion (Posa et al., 2013)(Hauser, 2014). Given an initial trajectory that may be non-optimal or even non-feasible, trajectory optimization methods can often quickly converge to a high-quality, locally-optimal solution.

We analyze the output trajectory using a novel graphical technique that we call "*Dynamic Coupling Map (DCM)*" that help gain insight into the motion of the system. Our ultimate goal for studying such systems is to understand problems of dynamic locomotion in both biological systems and in robotic systems.

The rest of the paper is structured as follow. Section (2) describes the Lagrangian dynamics of underactuated mechanical systems. A presentation of the trajectory optimization formulation is given in section (3). In section (4), we derive the dynamic coupling ellipsoid in both the unactuated acceleration space and the task space. The results of the numerical simulation and a discussion on the benefits of the Dynamic

Coupling Map as a graphical analysis tool to gain insight to the full acceleration capabilities of the underactuated system is given in(5). A discussion on possible extensions completes the paper.

2 LANGRANGIAN DYNAMICS OF UNDERACTUATED MECHANICAL SYSTEMS

Consider a dynamic system defined on a configuration manifold Q. let $(q, \dot{q}) = (q^1, \ldots, q^n, \dot{q}^1, \ldots, \dot{q}^n)$ denote local coordinates on the tangent bundle $\mathcal{T}Q$. We refer to $q, \dot{q}$, and $\ddot{q}$ as the vectors of generalized coordinates, generalized velocities, and generalized accelerations, respectively. Let the system possess a control input space of dimension $m < n$, where $u \in \mathbb{R}^m$ denote the vector of the control variables. Without loss of generality, we decompose the set of generalized coordinates $q = (q^1, \ldots, q^n) \in \mathbb{R}^n$ into $q = (q_p, q_a)$ where $q_p \in \mathbb{R}^{n-m}$, $q_a \in \mathbb{R}^m$ denote the passive degrees of freedom and the actuated degrees of freedom.

$$q = \begin{bmatrix} q_{p(n-m \times 1)} \\ q_{a(m \times 1)} \end{bmatrix} \in \Re^n \qquad (1)$$

We can then write the Euler-Lagrange equation of motion in a canonical form as

$$\begin{pmatrix} M_{pp} & M_{pa} \\ M_{pa}^T & M_{aa} \end{pmatrix} \begin{pmatrix} \ddot{q}_p \\ \ddot{q}_a \end{pmatrix} + \begin{pmatrix} \mathcal{N}_p(q, \dot{q}) \\ \mathcal{N}_a(q, \dot{q}) \end{pmatrix} = \begin{pmatrix} 0 \\ \tau \end{pmatrix} \quad (2)$$

where the joint space inertia matrix is decomposed into:

- M_{pp}: represents The inertia matrix for the system seen at the passive articulating subsystem

- M_{aa}: represents The inertia matrix of the active articulating subsystem

- M_{pa}: The inertial coupling term between the active and passive articulating subsystems

- $\ddot{q}_p$ is the second derivative of the floating base's pose (position and orientation) w.r.t time. While $\ddot{q}_q$ is the m-actuated joints acceleration.

- τ: The vector of the joint torques of the articulated system, assuming that articulated system is fully actuated.

- $\mathcal{N}_a(q, \dot{q})$: is the generalized bias force, it follows that it is the value that τ would have to take in order to produce zero joint acceleration, assuming that all the other joint accelerations are zero. Generalized bias force is a vector of force terms that account for Coriolis and centrifugal forces,

gravity. We assume that there exist no external wrenches, for the sake of the clarity of presentation.

- $\mathcal{N}_p(q, \dot{q})$: is the generalized bias force acting on the passive subsystem.

3 TRAJECTORY OPTIMIZATION

A trajectory optimization problem seeks to find the a trajectory for some dynamical system that satisfies some set of equality and inequality constraints constraints while minimizing some cost functional.

An abstraction of the Lagrangian dynamics in Eq.(2) can be written as a set of differential equations

$$\dot{x}(t) = f(x(t), u(t)) \qquad (3)$$

where $x = \begin{bmatrix} q \\ \dot{q} \end{bmatrix} \in \mathbb{R}^{2n}$ represent the system states, assuming the number of generalized coordinates equal to the number of generalized velocities. The input control vector $u \in \mathbb{R}^m$ and the transition function $f(.)$ defines the system evolution in time. Trajectory optimization problem seeks to find a finite-time input trajectory $u(t), \forall \in [0, t_f]$, such that a given criteria is minimized,

$$G = \phi(t_0, \mathbf{x}_0, t_f, \mathbf{x}_f) + \int_{t_0}^{t_f} g(t, x, u)\, dt \qquad (4)$$

where $\phi(.)$ and $g(.)$ are the intermediate and final cost function. The objective function can be written in terms of quantities evaluated at the ends of the phases only, in that case it is referred to as the Mayer form. If the objective function only involves an integral it is referred to as a problem of Lagrange, and when both terms are present it is called a problem of Bolza.

The optimization may be subject to a set of boundary constraints

$$\mathbf{b}_{min} < \mathbf{b}(t_0, \mathbf{x}_0) < \mathbf{b}_{max} \qquad (5)$$

$$\mathbf{b}_{min} < \mathbf{b}(t_f, \mathbf{x}_f) < \mathbf{b}_{max} \qquad (6)$$

In addition, Dynamic constraints, including the second order non-holonomic constraints, can be added as path constraints

$$\mathbf{c}_{min} < \mathbf{c}(t, \mathbf{x}(t), \mathbf{u}(t)) < \mathbf{c}_{max} \qquad (7)$$

Bounds on state variables and input control limits are added as

$$x_{min} \leq x(t) \leq x_{max} \qquad (8)$$

$$u_{min} \leq u(t) \leq u_{max} \qquad (9)$$

The result of the optimization is an optimal trajectory given by $[\mathbf{x}^*(t), \mathbf{u}^*(t)]$

To compute a feasible motion plan we transcribe the differential equation of the robot dynamics to algebraic equations and solve them through NonLinear Optimisation (NLP). (Betts, 2010) showed that that NLP can be interpreted as discrete approximations of the continuous optimal control problem. There are mature NLP solvers used in robotics; SNOPT (Gill et al., 2002) which is based on Sequential Quadratic Programming (SQP). The second solver is iPOPT (Wachter and Biegler, 2006) using the Interior Point Method. However, The complete description of the solvers and the algorithms used lies outside of the scope of this paper.

We employ direct method for transcribing and solving the optimal control problem. The solution to an optimal control problem via direct methods scales well to high-dimensional systems. In direct collocation, the optimization searches over a set of decision variables z, comprised by a vector of the states and control trajectories discretized over time at certain points or nodes, i.e., $z = [xk, uk]$, for $k = 1, ..., N$, where N represents the total number of nodes. Finally The NLP can be formulated as.

$$\underset{z}{minimize} \qquad G(z) \qquad (10)$$

$$subject\ to: \qquad l \leq \begin{pmatrix} z \\ c(z) \\ Az \end{pmatrix} \leq u \qquad (11)$$

In, direct collocation the input is represented as a piecewise-linear. function of time, and the state is piecewise-cubic. The values of the state and control at each knot point are the decision variables. The slope of state is prescribed by the dynamics at each knot point. The collocation points are the midvpoints of each cubic segment. The slope of the cubic at the collocation point is constrained to match the system dynamics at that point, as illustrated in figure(3). For more details the reader is referred to (Betts, 2010)(Betts, 1998).

4 DYNAMIC COUPLING MAP

4.1 Dynamic Coupling in the Unactuated Acceleration Space

Kinematic and dynamic coupling between the articulated system and the base is usually regarded as unwanted perturbation that degrades positioning accuracy and operational dexterity. In this work we attempt to exploit the dynamic coupling between the unactuated subsystem and its associated active articulated subsystem. we will start first by exploring the
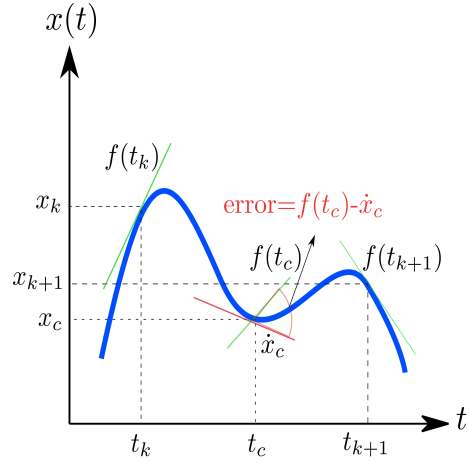
Figure 3: Illustration of the state trajectory discretization occurring in direct collocation optimization. System dynamics $f(t_c)$ are enforced to match the slope of the cubic $\dot{x}_c$ at the collocation point x_c.

relationship between the acceleration space of the unactuated subsystem and the torque space of the active articulating subsystem.

The dynamic equations of the system (2) can be decomposed into two main equations; one describing the dynamics of the passive free-floating base.

$$M_p\,\ddot{q}_p + M_{pa}\,\ddot{q}_a + \mathcal{N}_p = 0 \qquad (12)$$

and the second equation describing the dynamics of the articulated system

$$M_a\,\ddot{q}_a + M_{pa}^T\,\ddot{q}_p + \mathcal{N}_a = \tau \qquad (13)$$

For the sake of clarity, we dropped the dependence of the force bias terms $\mathcal{N}_{a,p}$ on $q, \dot{q}$.

Definition 4.1. *The underactuated mechanical system (2) is locally Strongly Inertially Coupled if and only if*

$$rank(M_{bm}(q)) = n - m \qquad for\ all\ q \in \mathcal{B}$$

where $\mathcal{B}$ is a neighborhood of the origin. The Strong Inertial Coupling is global if the rank condition holds for all $q \in Q$

the strong inertial coupling condition (Spong, 1998) requires that the number of active degrees of freedom be at least as great as the number of passive degrees of freedom.

Under the assumption of Strong Inertial Coupling we may compute a pseudo-inverse $M_{pa}^{\dagger}$ for M_{pa} as

$$M_{pa}^{\dagger} = M_{pa}^T (M_{pa} M_{pa}^T)^{-1} \qquad (14)$$

Then active joints generalized accelerations $\ddot{q}$ in (12) can be expressed as

$$\ddot{q}_a = -M_{pa}^{\dagger} M_p \ddot{q}_p - M_{pa}^{\dagger} \mathcal{N}_p \qquad (15)$$

By substituting (15) in (13), we can find a relation between the acceleration of the passive subsystem and its *acting surrounding*, which include; Joint torques, Nonlinear inertial forces, Gravity and wrench acting on the end points of the articulated system, if exists.

$$\ddot{q}_p \left(M_{pa}^T - M_a M_{pa}^\dagger M_p \right) - M_a M_{pa}^\dagger \mathcal{N}_p + \mathcal{N}_a = \tau \quad (16)$$

we finally express equation (16) as

$$\ddot{q}_p = \mathcal{Z}^\dagger \left(\tau + \widetilde{\mathcal{N}} \right) = \ddot{q}_{p_\tau} + \ddot{q}_{p_{bias}} \quad (17)$$

where we introduce the dynamic coupling factor $\mathcal{Z}^\dagger$ as

$$\mathcal{Z}^\dagger = \left(M_{pa}^T - M_a M_{pa}^\dagger M_p \right)^\dagger \quad (18)$$

$\mathcal{Z}$ is the Schur complement (Kolda and Bader, 2008) of the inertia coupling M_{bq} between the passive subsystem and the active articulating system We denote, as well, the bias term.

$$\widetilde{\mathcal{N}} = M_a M_{pa}^\dagger \mathcal{N}_p - \mathcal{N}_a \quad (19)$$

equation (17) provides an intuitive comprehension of the influence of different forces on the motion of the passive subsytem: $\ddot{q}_{p_\tau}$ is the acceleration of the passive subsystem due to the torques of the active articulated system, $\ddot{q}_{p_{bias}}$ is the acceleration due to gravity and non-linear inertial forces, and wrenches acting on the articulated system such as contact forces.

Furthermore, we note that the inverse of the dynamic coupling factor $\mathcal{Z}^\dagger$ act as transmission factor between the control input space τ and the acceleration space of the passive subsystem. $\mathcal{Z}^\dagger$ is configuration-dependent matrix. Thereby, it is possible to search for the configuration that maximizes the dynamic coupling factor which will result in a decrease in the effort expenditure. This formulation of the dynamic equation helps in analyzing the effects of these three sets of variables on the achievable set of free floating base acceleration.

4.2 Dynamic Coupling Ellipsoid

The goal of the Floating base dynamic coupling ellipsoid is to represent geometrically, in the acceleration space, the ensemble of the accelerations achievable by the unactuated subsystem. The torque limits at each actuator in the articulated system are assumed to be symmetrical, that is,

$$-\tau_{i,max} \le \tau_i \le \tau_{i,max} \quad (20)$$

The normalized joint torque vector $\tilde{\tau}$ can be expressed as

$$\tilde{\tau} = L^{-1}\tau \quad (21)$$

where the scaling matrix L is given by

$$L = diag(\tau_{1,max}, \tau_{2,max}, \ldots, \tau_{n,max}) \quad (22)$$

The control input space can then be represented as *m*-dimensional sphere defined by

$$\tilde{\tau}^T \tilde{\tau} \le 1 \quad (23)$$

By solving Eq.(17) and substituting in Eq.(23) we get the equation of an ellipsoid in the acceleration space of the passive subsystem.

$$(\ddot{q}_p - \ddot{q}_{p_{bias}})^T (\mathcal{Z}^\dagger L)^{-T} (\mathcal{Z}^\dagger L)^{-1} (\ddot{q}_p - \ddot{q}_{p_{bias}})^T \le 1 \quad (24)$$

which simplifies to

$$(\ddot{q}_p - \ddot{q}_{p_{bias}})^T \tilde{\mathcal{Z}} (\ddot{q}_p - \ddot{q}_{p_{bias}})^T \le 1 \quad (25)$$

where

$$\tilde{\mathcal{Z}} = \mathcal{Z}^T L^{-2} \mathcal{Z} \quad (26)$$

By applying singular value decomposition, $\tilde{\mathcal{Z}}$ can be decomposed into

$$\tilde{\mathcal{Z}} = U \Sigma V^T \quad (27)$$

where $U \in \mathbb{R}^{m \times m}$ and $V \in \mathbb{R}^{n \times n}$ are orthogonal matrices. The principal axis of the $n - m$-dimensional ellipsoid is determined by the eigenvectors u_i, while its length is specified by the corresponding eigenvalue $\sqrt{\sigma_i}$. Furthermore, the term $\ddot{q}_{bias}$ is responsible for translating the ellipsoid center from its origin.

4.3 Dynamic Coupling in the Task Space

In certain applications, it is more natural to reason about the underactuated mechanical system in the task space acceleration space, when it is more relevant than the generalized accelerations space. We extend the previous analysis to describe the dynamic coupling between the active subsystem and the task space, while taking into consideration the unactuated nature of the mechanical system.

let $X = \begin{bmatrix} x_1 & x_2 & \ldots & x_d \end{bmatrix}^T$ denote the *d*-dimensional task vector, which can represent the Cartesian position of the end effector of the manipulator or the center of mass of the underactuated system or any configuration dependent task can be formulated as $X = f(q)$. By taking the Taylor expansion of this mapping we derive the Jacobian that maps the task space velocities to the generalized velocities of the underactuated system.

$$\dot{X} = J(q)\dot{q} \quad (28)$$

The task space acceleration can be found by differentiating Eq.(28) with respect to time yielding

$$\ddot{X} = J(q)\ddot{q} + \dot{J}(q,\dot{q})\dot{q} \quad (29)$$

we partition further Eq.(29) into passive and active subsystems as follows

$$\ddot{X} = J_p \ddot{q}_p + J_a \ddot{q}_a + \dot{J}(q,\dot{q})\dot{q} \qquad (30)$$

From Eq.(13) we can express the generalized acceleration of the active subsystem function in torque as

$$\ddot{q}_a = \bar{\mathcal{Z}}(\tau - \mathcal{N}_a) \qquad (31)$$

where

$$\bar{\mathcal{Z}} = M_{pa}^T - M_{aa}M_{pp}^{-1}M_{pa} \qquad (32)$$

The generalized acceleration of the passive subsystem can also be expressed as

$$\ddot{q}_p = -M_{pp}^{-1}M_{pa}\ddot{q}_a - M_{pp}^{-1}\mathcal{N}_p \qquad (33)$$

By substituting Eq.(31) in Eq.(33) we get

$$\ddot{q}_p = -M_{pp}^{-1}M_{pa}(\bar{\mathcal{Z}}(\tau - \mathcal{N}_a)) - M_{pp}^{-1}\mathcal{N}_p \qquad (34)$$

To find the relationship between the Task space acceleration to the control input space, we substitute Eq.(34) and Eq.(31) in Eq.(29)

$$\ddot{X} = \mathcal{Z}^* \tau + \ddot{X}_{bias} \qquad (35)$$

where $\mathcal{Z}^*$ and $\ddot{X}_{bias}$ are defined as

$$\mathcal{Z}^* = J_a \bar{\mathcal{Z}} - J_p M_{pp}^{-1} M_{pa} \bar{\mathcal{Z}} \qquad (36)$$

$$\ddot{X}_{bias} = J_p M_{pp}^{-1} M_{pa} \mathcal{N}_p - J_p M_{pp}^{-1} \mathcal{N}_a - J_a \bar{\mathcal{Z}} \mathcal{N}_a + \dot{J}(q,\dot{q})\dot{q} \qquad (37)$$

Following the same procedure in 4.2 for deriving the dynamic coupling ellipsoid in the generalized acceleration space , we can define the dynamic coupling ellipsoid in the task space

$$(\ddot{X} - \ddot{X}_{bias})^T (\mathcal{Z}^* L)^{-T} (\mathcal{Z}^* L)^{-1} (\ddot{X} - \ddot{X}_{bias}) \leq 1 \quad (38)$$

5 EXPERIMENT RESULTS

5.1 Model Description

For the purpose of illustration, we focus our attention to the swing-up dynamic motion of the 'Gymnast' robot shown in figure (2). The Gymnast is a highly simplified approximation of an athlete swinging his body on a high bar. The model is composed of 3 links representing the arm, the trunk and the leg. All 3 links are connected by 1-DoF rotary joints. The arm is connected to the world through a passive joint, while the second and the third joint are active and torque controlled. Assuming symmetrical motion, we restrict our attention to the sagittal plane.

The inertial parameters used are; $m_1 = 1$ Kg, $m_2 = m_3 = 2$ Kg denoting the masses of the first, second and third link, respectively. The first link has a length of $l_1 = 1m$ while the second and third links have lengths of $l_2 = l_3 = 2m$. Density assumed to be homogeneous, thus $l_{c_1} = 0.5m$ and $l_{c_2} = l_{c_3} = 1m$ denotes the relative positions of the center of mass. The torque limits for actuators are given by $L = diag(10\,N.m, 10\,N.m)$

The robot is modeled using MIT toolbox Drake (Tedrake, 2014) in a Matlab environment. The optimization problem is solved using a non-linear optimization solver SNOPT based on Sequential Quadratic Program (SQP) algorithm.

5.2 Results

The non-linear optimization solver finds a local-optimal trajectory for the dynamic swing up motion of the Gymnast robot. Figure (4) shows a compilation of the motion from the down equilibrium position $q = \begin{bmatrix} q_1 & q_2 & q_3 \end{bmatrix}^T = \begin{bmatrix} 0 & 0 & 0 \end{bmatrix}^T$ to the up-right unstable equilibrium position $q = \begin{bmatrix} \pi & 0 & 0 \end{bmatrix}^T$. The first link is shown in blue, while the second and third links are shown in red and yellow, respectively. Figure (6) and figure (5) shows the evolution of the generalized position and velocities during swing up motion, respectively. We can note that although we have set an initial guess of the time span of the motion to be $t_0 = 6$ seconds the optimization achieved the goal configuration with an optimal time of $t^* \simeq 4$. Figure (7) shows the optimal torque control policy for the actuated subsystem, τ_2 & τ_3 in this case.

The Dynamic coupling analysis is depicted in Table(1), Table (2) & Table (3). Each column represents an instance of the motion with an interval of 0.3 seconds. The first row shows snapshots of the configurations of the 'Gymnast' robot during the swing-up trajectory. The second row shows only the shape of the corresponding dynamic coupling ellipsoids in the task space. In this case, it offers an intuitive Cartesian acceleration of the terminal organ representing the foot (colored in purple). The horizontal acceleration is depicted on the abscissa, while the vertical acceleration is depicted on the ordinate. The principal axis and scale of the dynamic coupling ellipsoid is determined by singular value decomposition of $(\mathcal{Z}^* L)^{-T} (\mathcal{Z}^* L)^{-1}$ in equation (38). The third row shows the trajectory of the dynamic coupling ellipsoid while taking into consideration the non-linear inertial forces. Unlike row 2 which shows the dynamic coupling ellipsoid centered at the origin, row 3 shows the displaced ellipsoid due to the contribution of the non-linear inertial forces $\ddot{X}_{bias}$ in equation (37). The vector of displacement from the instantaneous origin is represented by an arrow.

Table 1: Snapshots of the swing-up trajectory: The first row shows the configurations of the 'Gymnast' robot during the swing-up trajectory. The second row shows the shape of corresponding dynamic coupling ellipsoids. The Third row shows the trajectory of the dynamic coupling ellipsoid while taking into consideration the non-linear inertial forces. The first link with a passive joint is shown in blue. The second and third link with active joints are shown in red and yellow, rescpectively.
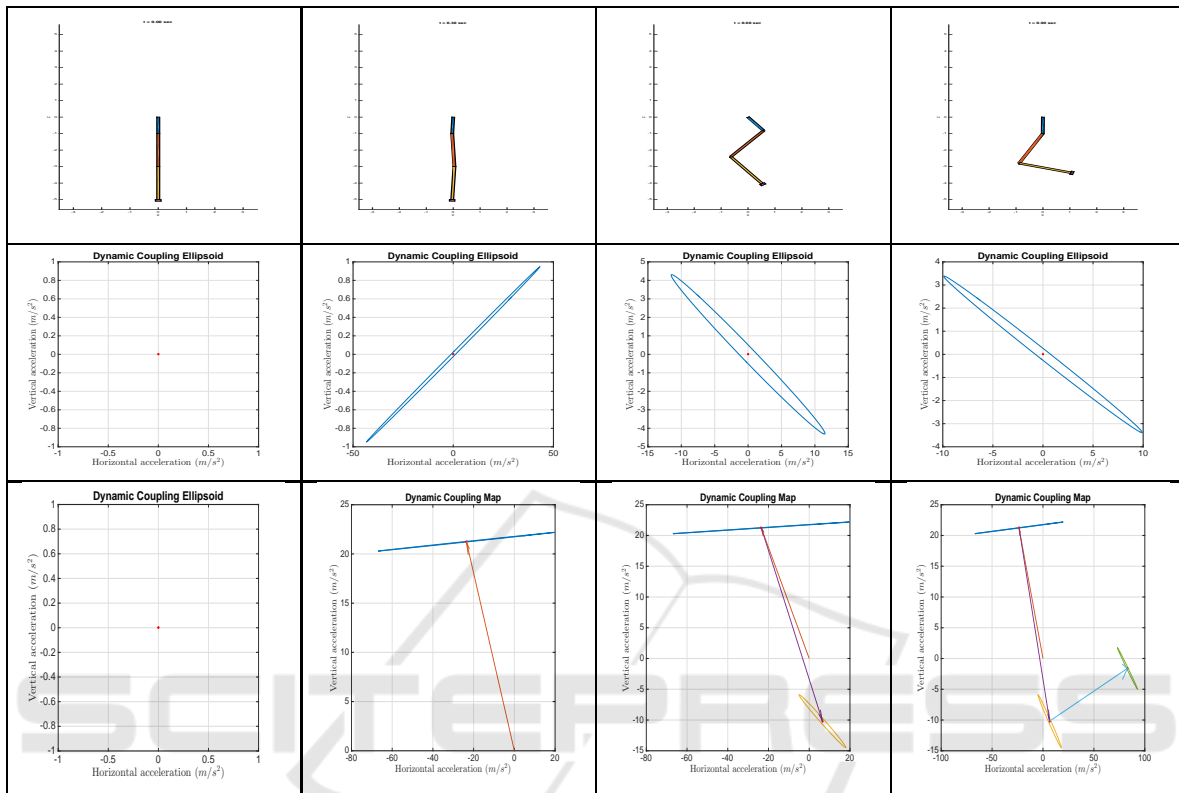
5.3 Discussion

Trajectory optimization proved to be an interesting approach to generate high quality dynamic motion despite its local optimality aspect. Moreover, its natural capacity to integrate all types of constraints (linear, nonlinear, complementarity problems), objective functions and application-related heuristics allowed it to gain traction in the robotics community. However, after many iterations, the optimization solver outputs a single local optimal trajectory without any insight into the nature of the given trajectory. The swing up motion example illustrates the emergence of nontrivial solution to the torque control, velocity and position trajectory from simple core principles (goal configuration, torque limit, dynamic model).

We use the Dynamic Coupling map (DCM) to analyze the dynamic motion given by the optimization. To facilitate the navigation and explanation of the DCM, let the location of each cell in table (1) be given by the triplet (t, r, c), where t r and c corresponds to the number of table, row and column, respectively. The 'Gymnast' starts from an equilibrium position depicted in cell(1,1,1), where the dynamic coupling el-
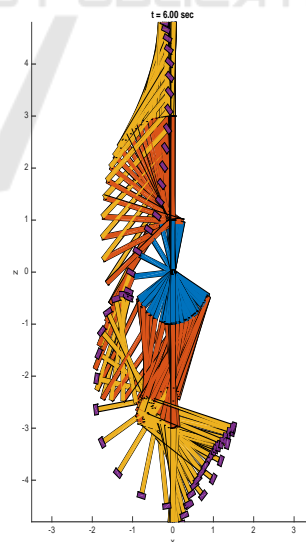
Figure 4: Local-optimal swing-up motion.

lipsoid in the task space representing the maximum acceleration capacity of the terminal organ (shown in purple) is shown in cell(1,2,1). Since the starting configuration is singular the Jacobian-dependent el-

Table 2: Continued.
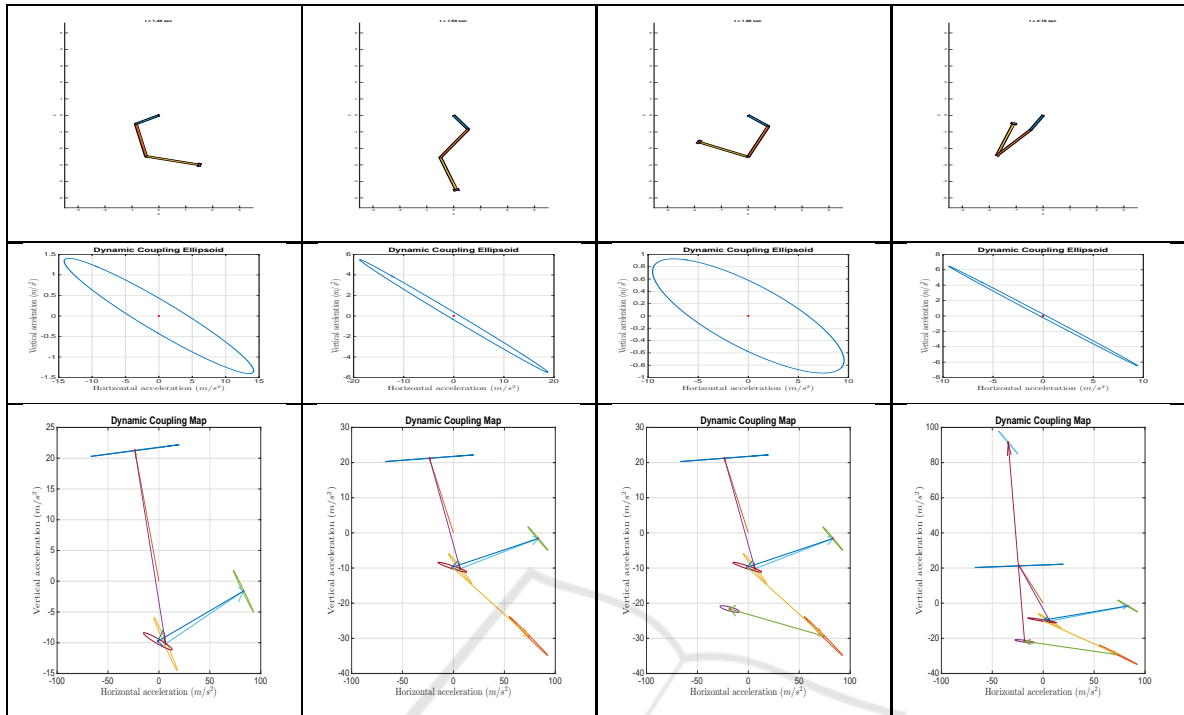
Table 3: Continued.
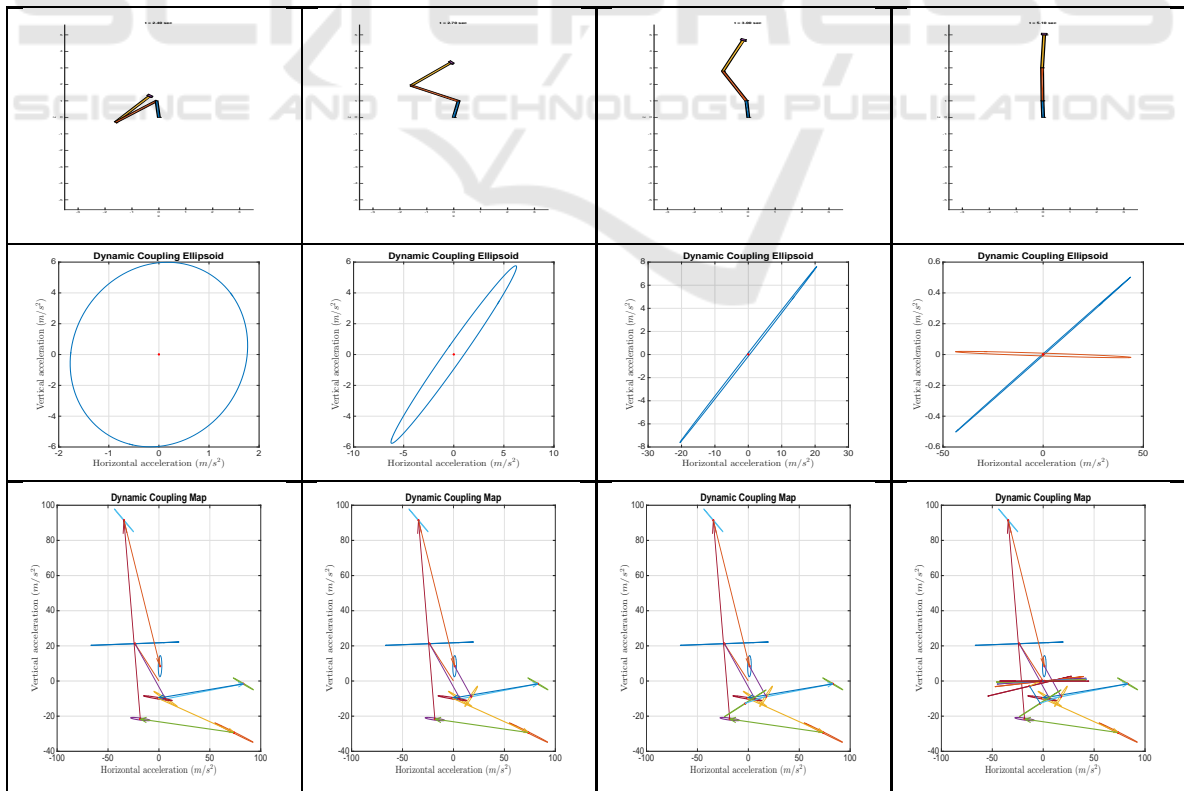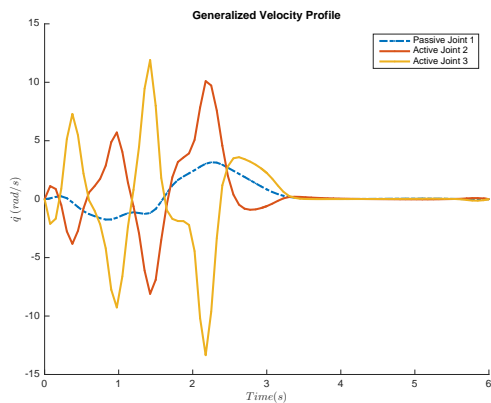
Figure 5: Local-optimal Generalized Velocities Profile for the swing-up motion.
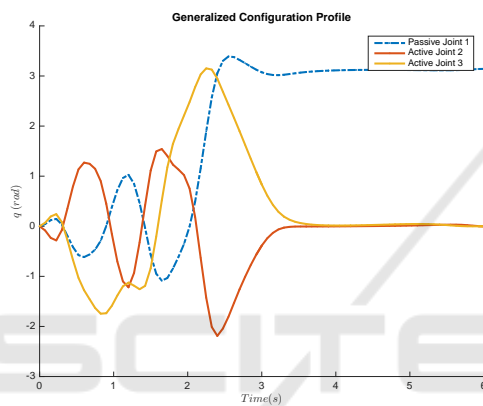
Figure 6: Local-optimal Generalized Coordinates Profile for the swing-up motion.
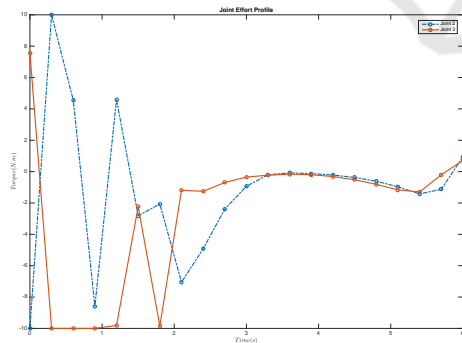
Figure 7: Local-optimal Torque Control Profile for the swing-up motion.

lipsoid fails to give any valuable information at this configuration, except that it is singular. The Gymnast starts applying torque at the shoulder and the knee (Joint 2 & 3). However, it is clear from figure (7) that the Gymnast hits already the torque limits at 10 (Nm). The Dynamic Coupling ellipsoid (DCE), depicted in cell(1,2,2), shows the limited capacity of the underactuated robot to accelerate in the vertical

direction (limited at a range of $+/-1\,m/s^2$) while most of the actuation effort can be transmitted in the horizontal direction range ($+/-50\,m/s^2$). We observe that DCE is almost degenerate due to the near singular configuration. In other words, it means that the actuators solely fails to move the underactuated robot directly to the upright configuration. However, in the following frames the robot exploit the passive dynamics by swinging to acquire a vertical acceleration capacity beyond what is provided by the actuators. By inspecting cell(1,3,2), we can see that the DCE shape, determined by actuator torque limits, doesn't tell the whole story. That is because the DCE is shifted from its origin by the vector $\ddot{X}_{bias}$ which is influenced by the velocity-dependent nonlinear inertial forces. Cell(1,3,2) shows that the DCE origin is shifted to $20\,m/s^2$ due to the nonlinear inertial forces. In the following frames, we find that the optimization starts exploiting this displacement to increase the vertical acceleration capacity. Cell(2,3,3) shows that optimization was able to increase the vertical acceleration to about $90\,m/s^2$ thanks to the exploitation of the velocity-dependent non-linear inertial forces. Another interesting observation, is that at this specific instant at $t = 2.2s$ in figure (7), we can see that the robot reduce its independence on the torque effort and start exploiting its own passive dynamics to pursue its movement towards the goal configuration. In 3, we observe that the robot starts stabilizing its motion by decelerating towards the goal configuration with zero velocity.

The current presentation of the Dynamic Coupling Map highlight the importance of the velocity-dependent nonlinear inertial forces to achieve highly dynamic motions. The DCM maps the interplay of the input control space and the dynamic coupling to achieve a desired acceleration. Although the current presentation provides 'a posteriori' graphical analysis of the dynamic capability of underactuated manipulators, it raises an interesting question about the possibility of exploiting this map to design an optimal trajectory 'a priori'.

6 CONCLUSIONS AND FUTURE WORK

Motivated by the agile motion of humans and animals in nature, we have employed Direct collocation trajectory optimization to find optimal control policy for the swing up motion of a gymnast on high bar. We have introduced the Dynamical Coupling Map (DCM), a graphical technique, to gain insight into the output trajectory of the optimization and analyze the

acceleration capability of underactuated mechanical systems. We highlighted the importance of the effects of the nonlinear inertial forces on the acceleration limits of underactuated system.

A perspective of this work, is to extend the current analysis to floating-base systems, a special class under actuated mechanical systems driven by the interaction with the environment as well as the dynamic coupling of its articulating system.

REFERENCES

Arai, H., Tanie, K., and Shiroma, N. (1998). Nonholonomic control of a three-DOF planar underactuated manipulator. *IEEE Trans. Robot. Autom.*, 14(5):681–695.

Åström, K. J. and Furuta, K. (2000). Swinging up a pendulum by energy control. *Automatica*, 36(2):287–295.

Betts, J. T. (1998). Survey of Numerical Methods for Trajectory Optimization. *J. Guid. Control. Dyn.*, 21(2):193–207.

Betts, J. T. (2010). *Practical Methods for Optimal Control and Estimation Using Nonlinear Programming*.

Gill, P. E., Murray, W., and Saunders, M. A. (2002). SNOPT: An SQP Algorithm for Large-Scale Constrained Optimization. *SIAM J. Optim.*, 12(4):979–1006.

Hauser, J. and Murray, R. M. (1990). Nonlinear controllers for non-integrable systems: the Acrobot example. *1990 Am. Control Conf.*, (1):669–671.

Hauser, K. (2014). Fast interpolation and time-optimization with contact. *Int. J. Rob. Res.*, 33(9):1231–1250.

Ibuki, T., Sampei, M., Ishikawa, A., and Nakaura, S. (2015). Jumping Motion Control for 4-Link Robot Based on Virtual Constraint on Underactuated Joint. *Sc.Ctrl.Titech.Ac.Jp*, pages 1–6.

Kolda, T. G. and Bader, B. W. (2008). Tensor Decompositions and Applications. *SIAM Rev.*, 51(3):455–500.

Kurazume, R. and Hasegawa, T. (2002). A new index of serial link manipulator performance combining dynamic manipulability and manipulating force ellisoids. 1(8).

Lam, S. and Davison, E. (2006). The real stabilizability radius of the multi-link inverted pendulum. *Am. Control Conf. 2006*, (2):1814–1819.

Libby, T., Moore, T. Y., Chang-Siu, E., Li, D., Cohen, D. J., Jusufi, A., and Full, R. J. (2012). Tail-assisted pitch control in lizards, robots and dinosaurs. *Nature*, 481(7380):181–184.

Luca, A. D. and Oriolo, G. (2002). Trajectory Planning and Control for Planar Robots with Passive Last Joint. *Int. J. Rob. Res.*, 21(5-6):575–590.

Lynch, K. and Mason, M. (1996). Dynamic underactuated nonprehensile manipulation. *Proc. IEEE/RSJ Int. Conf. Intell. Robot. Syst. IROS '96*, 2:889–896.

Nagarajan, U., Kantor, G., and Hollis, R. (2013). Integrated motion planning and control for graceful balancing mobile robots. *Int. J. Rob. Res.*, 32(9-10):1005–1029.

Olfati-Saber, R. (2001). Nonlinear Control of Underactuated Mechanical Systems with Application to Robotics and Aerospace Vehicles. page 307.

Patel, A. and Braae, M. (2013). Rapid turning at high-speed: Inspirations from the cheetah's tail. *IEEE Int. Conf. Intell. Robot. Syst.*, pages 5506–5511.

Posa, M., Cantu, C., and Tedrake, R. (2013). A direct method for trajectory optimization of rigid bodies through contact. *Int. J. Rob. Res.*, 33(1):69–81.

Shkolnik, A. and Tedrake, R. (2008). High-dimensional underactuated motion planning via task space control. *2008 IEEE/RSJ Int. Conf. Intell. Robot. Syst. IROS*, pages 3762–3768.

Spong, M. W. (1995). Swing up control problem for the acrobot. *IEEE Control Syst. Mag.*, 15(1):49–55.

Spong, M. W. (1998). Underactuated mechanical systems. *Control Probl. Robot. Autom. Springer*, pages 135–150.

Tamegaya, K., Kanamiya, Y., Nagao, M., and Sato, D. (2008). Inertia-coupling based balance control of a humanoid robot on unstable ground. *2008 8th IEEE-RAS Int. Conf. Humanoid Robot. Humanoids 2008*, pages 151–156.

Tedrake, R. (2014). Drake: A planning, control, and analysis toolbox for nonlinear dynamical systems.

Todorov, E. (2004). Optimality principles in sensorimotor control. *Nat. Neurosci.*, 7(9):907–15.

Wachter, A. and Biegler, L. T. (2006). *On the implementation of an interior-point filter line-search algorithm for large-scale nonlinear programming*, volume 106.

Wieber, P.-B. (2005). Some comments on the structure of the dynamics of articulated motion. *Ruperto Carola Symp. Fast Motions Biomech. Robot.*

Wieber Pierre-Brice, Tedrake Russ, K. S. (2015). *Modeling and Control of Legged Robots*. Springer, 2nd ed edition.

Xin, X. (2013). On simultaneous control of the energy and actuated variables of underactuated mechanical systems-example of the acrobot with counterweight. *Adv. Robot.*, 27(12):959–969.

Xin, X. and Kaneda, M. (2007a). Analysis of the energy-based swing-up control of the Acrobot. *Int. J. Robust Nonlinear Control*, 17(16):1503–1524.

Xin, X. and Kaneda, M. (2007b). Design and analysis of swing-up control for a 3-link gymnastic robot with passive first joint. *Proc. IEEE Conf. Decis. Control*, 23(6):1923–1928.